https://doi.org/10.5194/egusphere-2025-666
Preprint. Discussion started: 21 February 2025

Southern Annular Mode Persistence and Westerly Jet: A Reassessment Using High-Resolution Global Models

Ting-Chen Chen[1], Hugues Goosse[1], Matthias Aengenheyster[2], Kristian Strommen[3], Christopher Roberts[2], Malcolm Roberts[4], Rohit Ghosh[5], Jin-Song von Storch[6], Stephy Libera[1]

[1]Earth and Life Institute, Université Catholique de Louvain, Ottignies-Louvain-la-Neuve, Belgium
[2]European Centre for Medium Range Weather Forecasting (ECMWF), Reading, United Kingdom
[3]Department of Atmospheric, Oceanic, and Planetary Physics, University of Oxford, Oxford, UK
[4]Met Office Hadley Centre, Exeter, United Kingdom
[5]Alfred Wegener Institute Helmholtz Centre for Polar and Marine Research, Bremerhaven, Germany
[6]Max-Planck Institute for Meteorology, Hamburg, Germany

Correspondence to: Stephy Libera (stephy.libera@uclouvain.be)

Abstract. This study evaluates the performance of high-resolution (grid sizes of 9–28 km for the atmosphere; 5–13 km for the ocean) global simulations from the EERIE project in representing the persistence of the Southern Annular Mode (SAM), a critical driver of Southern Hemisphere climate variability. Using the decorrelation timescale of the SAM index (τ), we compare EERIE coupled and atmosphere-only (AMIP) simulations with CMIP6 and ERA5 datasets. EERIE coupled simulations improve the long-standing biases in SAM persistence, especially in early summer, with τ values of 9–17 days compared to CMIP6's 9–32 days. This improvement generally correlates with a more accurate climatological jet latitude (λ_0) distribution in EERIE simulations than in CMIP6, but such a correlation is not robust within EERIE AMIP simulations with a well-represented jet location, suggesting other factors in play. With prescribed SSTs, EERIE AMIP show even smaller biases in both τ and λ_0 than EERIE coupled runs, highlighting the critical role of SST representation. Using the same AMIP model, finer grids (9 km vs. 28 km) can further reduce τ, but the underlying cause remains unclear, likely because of potential compensation between different processes. Sensitivity experiments filtering ocean mesoscale features in SST boundary conditions suggest that mesoscale processes enhance SAM persistence by ~2 days in early summer, though this effect is clear in ensemble means at 28 km but not in the single 9-km runs. We also show that the atmospheric eddy feedback strength is a better indicator than λ_0 to infer the SAM persistence, although the metric alone does not fully explain the τ differences

https://doi.org/10.5194/egusphere-2025-666
Preprint. Discussion started: 21 February 2025

across SST scenarios. These findings underscore the interplay of dynamic processes influencing SAM persistence and offer insights for advancing global climate model performance.

1 Introduction

Over the extratropical Southern Hemisphere, the daily- to decadal climate variability is dominated by the Southern Annular Mode (SAM), a mode of natural variability manifested in the large-scale oscillation of atmospheric mass between mid- and high-latitudes and hence the north-southward shift and intensity change of the eddy-driven jet in the midlatitudes (e.g., Fogt and Marshall, 2020). This internal variability both influences and is influenced by the atmospheric circulation, affecting regional temperature and precipitation patterns, sea ice extent, and ocean circulation, with consequences for global heat and carbon redistribution (e.g., Doddridge and Marshall, 2017; Gillett et al., 2006; Lefebvre and Goosse, 2005; Lenton and Matear, 2007; Lovenduski and Gruber, 2005).

As inferred by its name “annular”, the spatial structure of SAM is approximately “ring-shaped” when viewed from above the South Pole and is nearly barotropic in the vertical direction (Gerber et al., 2010). During the positive phase of SAM, lower air pressure anomalies overlay Antarctica while higher pressure anomalies spread over the mid-latitudes, and such anomalous pressure distribution indicates a strengthening and poleward shifting of the westerly jet that climatologically sits at around 50°S (Lim et al., 2013). While the SAM can, to a first approximation, be described from a zonal-mean perspective, its structure can deviate from the zonal mean and vary across different timescales, affected by factors such as the seasonal cycle of midlatitude jet (atmospheric eddy activity), sea surface temperature (SST) variability, tropical oscillations such as the El Niño-Southern Oscillation (ENSO), stratosphere-troposphere interactions and so on (e.g., Campitelli et al., 2022; Ding et al., 2012; Fogt and Marshall, 2020; Karoly, 1989). On the seasonal scale, SAM is overall more zonally symmetric in austral summer (DJF) but exhibits asymmetric wavenumber 3 components when entering spring (MAM) and summer (JJA). Readers interested in a comprehensive review of the SAM literature are encouraged to consult Fogt and Marshall (2020) and Thompson et al. (2011).

An important characteristic of SAM is its temporal persistence, referring to how long a given phase of the SAM (positive, negative or neutral) tends to last before transitioning. It is often measured as the

https://doi.org/10.5194/egusphere-2025-666
Preprint. Discussion started: 21 February 2025

decorrelation timescale (e-folding timescale) which indicates the average duration over which the SAM index remains strongly correlated with its past values. While global climate models (GCMs) have shown good skills in capturing the spatial structure of SAM variability, a long-standing common challenge for GCMs is that they tend to overestimate the SAM persistence during the austral summer. Based on global reanalysis data, the SAM decorrelation timescale is found to be approximately 10 days on annual mean and is a couple of days higher in early summer (November–January; NDJ), during which period GCMs typically show values that are two to three-times larger (Bracegirdle et al., 2020). Many studies have found a strong dependency between the SAM persistence bias and the bias in the climatological westerly jet location (e.g., Kidston and Gerber, 2010; Simpson et al., 2013; Simpson and Polvani, 2016; Son et al., 2010), that is, GCMs showing too persistent SAM tend to be associated with a too equatorward-placed tropospheric westerly jet. A possible explanation for such a relationship is that the structure of the climatological jet can affect the tropospheric eddy-mean flow feedback, the process by which small-scale atmospheric eddies interact with large-scale climate anomalies to amplify them, and models with lower latitude jets exert stronger feedback to maintain SAM (Codron, 2005; Simpson and Polvani, 2016).

However, the climatological position of the midlatitude jet is not the only factor for the overly persistent SAM variability in GCMs. Simpson et al. (2013) performed a series of experiments with nudging and bias correcting procedures using a stratosphere-resolving GCM, the Canadian Middle Atmosphere Model (CMAM). They found that the SAM persistence bias remains even when the representation of the climatological tropospheric winds is artificially improved. Similar conclusions are obtained when another common bias for the overly-persistent summertime SAM —specifically, the delayed breakdown of the stratospheric vortex— was manually nudged toward the reanalysis-based seasonal climatology. Based on these results, they suggested that a substantial proportion of the SAM timescale bias arises from “internal” tropospheric dynamics, specifically the atmospheric eddy-mean flow feedback.

Such a feedback mechanism assumes that the shifted midlatitude jet associated with the positive/negative SAM acts as a source of eddies. When eddies propagate away from the source region before breaking, convergence of eddy vorticity flux is produced in the upper troposphere. Such eddy vorticity flux convergence can reinforce the shifted jet by enhancing the baroclinicity through adiabatic

https://doi.org/10.5194/egusphere-2025-666
Preprint. Discussion started: 21 February 2025

heating/cooling associated with the induced secondary circulation, thus extending the SAM persistence against dissipation from surface friction. Within this framework, Barnes and Hartmann (2010) performed a budget analysis of the relative vorticity tendency equation in a global reanalysis. Their analysis showed that this feedback is present across the hemisphere in austral summer but lacking over the western Pacific in winter due to a weaker climatological midlatitude jet in that region. Such a seasonal variation appears to explain the longer SAM timescale in summer than in winter. Following a similar concept, Simpson et al. (2013) performed momentum budget analysis of the vertically averaged and zonally averaged zonal wind associated with SAM and confirmed that the maintenance of SAM anomalous wind is dominated by the eddy momentum flux convergence that compensates the negative contribution by friction. They also showed that the overly persistent SAM is highly correlated (coefficient of 0.83) with the too strong total eddy feedback during the summer season in the Coupled Model Intercomparison Project Phase 5 (CMIP5) climate models.

As GCMs improve in their representation of physics, resolution, and overall complexity, some advancements have been made in reducing biases associated with SAM persistence and the climatological jet latitude. Compared to earlier versions of CMIP models (e.g., CMIP3, CMIP5), noticeable reductions in these biases have been reported. Bracegirdle et al. (2020) found that the ensemble-mean bias in the westerly jet latitude decreased from 1.9° in CMIP5 to 0.4° in CMIP6 on an annual mean basis. Consistently, the early-summertime SAM persistence was reduced from approximately 30 days in CMIP5 to 20 days in CMIP6. Nevertheless, the SAM decorrelation timescale remains systematically biased. While higher resolution is generally regarded as beneficial, it is worth exploring whether additional improvements are achievable by further increasing the resolution or if other factors become increasingly significant when the resolution has reached beyond a sufficiently high level.

This potential role of an increase in resolution in reducing the biases in SAM persistence and the relationship with the mean-state westerly jet is investigated here in new experiments conducted as part of the Horizon Europe project European Eddy-Rich Earth System Models (EERIE) (M. J. Roberts et al., 2024a). A distinctive feature of the high-resolution atmosphere-ocean coupled Earth System Models (ESMs) built under EERIE is their adoption of high oceanic resolutions to explicitly represent ocean

https://doi.org/10.5194/egusphere-2025-666
Preprint. Discussion started: 21 February 2025

mesoscale processes, which have been increasingly recognized as critical for weather and climate simulation in recent studies (e.g., Busecke and Abernathey, 2019; Chassignet and Xu, 2021; Hewitt et al., 2020). In addition to the development of new coupled models, EERIE also includes a suite of atmosphere-only simulations and idealized experiments to facilitate exploration of the atmosphere response to the ocean mesoscales by excluding effects attributed to the air-sea coupling and SST biases. Those experiments will allow disentangling the role of the explicit resolution of the eddies compared to the one of increasing the model resolution. The data sources and diagnostics are detailed in Sections 2 and 3, respectively, followed by the results in Section 4 and the conclusions in Section 5.

2 Data

2.1 EERIE models & simulations

Running from January 2023 to December 2026, the EERIE project aims to build new generations of ESMs run at "eddy-rich resolution" (note that the "eddy" here refers to ocean eddies), which explicitly resolve ocean mesoscale processes with scales of 10–100 km. Crucial components at this scale include the ocean eddies (analogous to cyclones in the atmosphere) and boundary/frontal currents. EERIE will deliver simulations over multi-centennial timescales centered on four global coupled ESMs and two atmosphere-only models, with an overarching objective to reveal and to quantify the role of ocean mesoscales in shaping the climate trajectory over seasonal to centennial time scales, regionally and globally (European Commission, 2022). The simulations are organized in two phases, with the Phase 1 providing guidance for the planning of Phase 2.

2.1.1 Coupled simulations

This study evaluates the preliminary EERIE Phase 1 simulations based on their regridded output on a 0.25° ×0.25° grid (Wachsmann et al., 2024). A detailed description of the EERIE models can be found in M. J. Roberts et al., (2024a), and here we briefly summarizes the simulations used in the current study (Table 1). We analyze five coupled simulations in total: four conducted following a protocol similar to the CMIP6 HighResMIP (High Resolution Model Intercomparison Project; Haarsma et al., 2016), using either the IFS-FESOM2 or ICON models, and one following similar protocol as CMIP6

https://doi.org/10.5194/egusphere-2025-666
Preprint. Discussion started: 21 February 2025

DECK (Diagnostic, Evaluation and Characterization of Klima; Eyring et al., 2016) with the HadGEM3-GC5-EERIE model. HighResMIP differs from CMIP6 DECK primarily in its use of 1950s' climate conditions instead of 1850s' as the initial state and a shorter spin-up (~50 years) due to the computational demands of high-resolution models. Using the IFS-FESOM2 model, we analyze selected segments of the spin-up and control runs (referred to as *1950spinup* and *1950control*), both conducted under fixed 1950 forcings. The analyzed segments vary in length depending on data availability, as detailed in Table 1. Additionally, we examine a portion of the historical simulation covering 1950–1969. For the ICON model, only the *1950spinup* run is available. For the HadGEM3 model, we investigate the pre-industrial control simulation *(piControl*) forced by 1850 conditions.

While these simulations cover different time periods, we do not expect these differences to significantly impact the evaluation of specific model performance in SAM persistence, as linear trends and a slowly varying climatology are removed in the SAM-related diagnostics. However, it should be borne in mind that this removal may not fully eliminate all non-stationary features in the second moments. Therefore, when evaluating EERIE runs against the ERA5 reanalysis (Section 2.2), a fairer comparison would be based on a similar earlier period, but the best available option starts from 1958, as observation in the Southern Hemisphere were sparse before then.

Table 1. EERIE simulations analyzed in the current study.

Institution	Alfred Wegener Institute (AWI)	Max Planck Institute (MPI-M)	Met Office (MO)	European Centre for Medium-range Weather Forecasting (ECMWF)
	Coupled atmosphere-ocean models (eddy-rich)			Atmospheric model
System name	IFS-FESOM2	ICON	HadGEM3-GC5-EERIE	IFS
Model components	IFS CY48R1, FESOM2, FESIM2	ICON-A, ICON-O	UM, NEMO4.0.4, SI3	IFS CY48R1
Atmos. grid (km)	Tco1279 (~9 km)	R2B8 (~10 km)	N640 (~20 km at 50N)	Tco1279 (~9 km) Tco399 (~28 km)* *five ensemble members
Atmos. vertical levels (model top)	137 (0.01 hPa)	90 (0.01 hPa)	85 (85 km)	137 (0.01 hPa)
Ocean res (km)	NG5 (~13-5 km)	R2B9 (~5 km)	eORCA12 (~8 km)	-

https://doi.org/10.5194/egusphere-2025-666
Preprint. Discussion started: 21 February 2025

Ocean vertical levels	70	72	75	-
Protocol	CMIP6 HighResMIP		CMIP6 DECK	HighResMIP2
Simulations (analyzed segments length)	1950spinup (31 yrs) 1950control (20 yrs) Historical (1950–1969)	1950spinup Cycle 2 (11 yrs)	piControl (30 yrs)	Historical (1980–2023)

2.1.2 Atmosphere-only simulations & sensitivity experiments

The EERIE AMIP simulations were performed for the historical period of 1980–2023 following the HighResMIP2 highresSST-present experimental design (M. J. Roberts et al., 2024b). The simulations were produced with the IFS model, tested with two model grid sizes (~28 km and ~9 km), and the higher-resolution configuration is identical to the atmosphere component of the coupled IFS-FESOM2 (Table 1). One member has been performed at the 9-km resolution, but the 28-km simulations are supplemented with five ensemble members to represent a range of model uncertainty or noise. These ensembles are generated by perturbing the atmospheric initial conditions for January 1, 1980, using the same methodology employed in operational ECMWF ensemble forecasts (C. Roberts et al., 2024a).

The prescribed boundary conditions include the daily-mean SST reanalysis from the European Space Agency Sea Surface Temperature Climate Change Initiative (ESA CCI SST v3) and the daily-mean sea-ice concentration from the European Organisation for the Exploitation of Meteorological Satellites (EUMETSAT) Ocean and Sea Ice Satellite Application Facility (OSI-SAF), both retrieved on a $0.05° \times 0.05°$ grid. External radiative forcings are generally specified following CMIP6/HighResMIP protocols, and the specificity can be found in C. Roberts et al. (2024a).

Taking the IFS-AMIP simulations as the reference (ObsSST), a series of idealized experiments with the SST boundary condition modified are carried out as part of the EERIE project to enable exploration of the response of the atmosphere to the extratropical SST ocean mesoscale features (C. Roberts et al., 2024b). Two types of modifications are designed. One is the NoFronts experiment, in which the quasi-stationary features in the extratropics are smoothed out by applying a spatial low-pass filter to the climatological mean field of SST. The other is the NoEddies experiment, with the transient oceanic eddy features removed from the SST boundary conditions with the same low-pass filter but applied to

https://doi.org/10.5194/egusphere-2025-666
Preprint. Discussion started: 21 February 2025

the SST anomaly field (difference from the climatological mean). Sea ice cover remains unchanged in all experiments. We emphasize that such design of NoEddies or NoFronts experiments only allows us to test the direct thermodynamic impact from ocean mesoscales (as reflected in SSTs) but not their relative winds-currents effects (wind stress feedback; or called current feedback).

The filter being employed is a Gaussian filter from the GCM-Filters Python package (Loose et al., 2022). The filter length scale is set to be $20L_R$ with a lower and higher limit of 30 km and 700 km, respectively, where L_R is the spatially varying climatological Rossby radius in the ocean. While a filter depending on a smaller L_R at high latitudes can effectively remove the smaller oceanic eddies there, it also removes the larger-scale tropical instability waves near the equator as L_R reaches maximum. The latter consequence may obscure the interpretation on the impact of the targeted extratropical ocean mesoscales due to the tropical-extratropical teleconnections. To avoid this, low-latitude areas are masked out from the filtering with the function with values ranging from 0 to 1: $M(\lambda) = \frac{1}{2}\left(\tanh\left(\frac{|h-\lambda|}{s}\right)+1\right)$, where h= 10 determines the latitude where the M value is halved (0.5) and s=3 scales the steepness of the masking function. Like the reference simulations, the NoEddies experiment is run with two model grid sizes of ~28 km (five ensemble members) and ~9 km (one member), and the NoFronts setup is only performed for the 28-km ensemble. For more details of the experimental design, we refer readers to (C. Roberts et al., 2024b).

2.2 CMIP6 models & ERA5 reanalysis

For the diagnostics of SAM persistence and westerly jet characteristics, the CMIP6 models are used to compare with EERIE models. We utilize the CMIP6 historical simulations from the first ensemble member that provide outputs of daily geopotential at 500-hPa level and monthly zonal wind at 850 hPa. A total of 31 simulations are available, and only the period of 1980-2014 is extracted to ensure a uniform data length. All CMIP6 outputs are regridded to a uniform $1° \times 1°$ grid with the bilinear interpolation before performing the analysis. As a proxy of observation, we use the global reanalysis dataset ERA5 (Hersbach et al., 2020) for the same variables and a total period from 1958 to 2023. The chosen period of ERA5-based analysis will be adjusted to align with the corresponding period of the

https://doi.org/10.5194/egusphere-2025-666
Preprint. Discussion started: 21 February 2025

target simulation for comparison. While we analyze ERA5 on the commonly distributed 0.25° ×0.25° grid, we have tested the impact with regridding it to the 1° ×1° grid and find no notable changes in our results.

3 Diagnostics

For the overall assessment of model performance, the diagnostics described in subsections 3.1 and 3.2 below are applied to all available CMIP6 historical and EERIE simulations. Due to the limited accessibility of the EERIE data at the time of writing, diagnostics in subsections 3.3 and 3.4 are only performed on the EERIE atmosphere-only sensitivity experiments to provide more insights on the tropospheric mechanisms critical to the SAM persistence.

3.1 SAM persistence timescale

Some variations exist in the definition of the SAM across the literature (Ho et al., 2012), and its persistence estimation may be sensitive to the methods employed. While many studies adopt similar methodological concepts, the details are often not fully transparent. To ensure clarity, we provide a step-by-step explanation of our approach. Note that SAM is a rather barotropic feature, so even though some traditional definitions consider the vertical averaged field, we have chosen to follow Bracegirdle et al. (2020) using a single level for simplicity.

We define the SAM as the first empirical orthogonal function (EOF) of daily zonal-mean geopotential anomalies on the 500-hPa level for the region south of 20°S (Bracegirdle et al., 2020). The anomalies are calculated based on Gerber et al. (2010). First, a time series of 500-hPa zonally mean $\bar{\Phi}(\lambda,t)$ is taken, where λ and t refer to latitude and time at daily intervals, respectively, and the bar indicates zonal average. Then, for each day, we subtract the global mean of 500-hPa geopotential from $\bar{\Phi}(\lambda,t)$ at each latitude, and the resulting data is linearly detrended. Lastly, a slowly varying climatology $\widetilde{\Phi}(\lambda,t)$ is subtracted to remove the seasonal cycle and the low-frequency nonlinear trends associated with known external forcings such as the ozone hole formation/recovery and global warming signal. The $\widetilde{\Phi}(\lambda,t)$ is derived in two steps: 1) Applying a 60-day low pass filter to the detrended $\bar{\Phi}(\lambda,t)$ along the t axis, which

https://doi.org/10.5194/egusphere-2025-666
Preprint. Discussion started: 21 February 2025

leaves us the seasonal-scale variations. 2) Then, for the same date in a calendar year, a 30-year low-pass filter is applied. If the data spans less than 30 years, the averaging of all available years for that same calendar date is performed, and hence $\widetilde{\Phi}(\lambda,t)$ is a fixed annual cycle that repeats across years.

The resultant anomalies $\overline{\Phi'}(\lambda,t)$ reflect the internal/natural variability. We can then obtain SAM as the first EOF of $\overline{\Phi'}(\lambda,t)$ over 20–90°S. For the computation of EOFs, $\overline{\Phi'}(\lambda,t)$ is weighted by $\sqrt{\cos(\lambda)}$ to account for the decreasing distance between meridians toward the pole. The resultant leading EOF $\mathbf{e}(\lambda)$ represents the spatial patterns of SAM, and its corresponding principal component time series PC(t) is referred to "SAM index", expressed in normalized form with zero mean and unit variance (Fig. 1a-b).

To quantify the temporal persistence of SAM, the decorrelation time scale is computed as the e-folding timescale of the autocorrelation function of the SAM index. Following the procedure in Simpson et al. (2013), we first calculate the autocorrelation function as

$$\mathrm{ACF}(d,l) = \frac{\sum_{y=1}^{N-1} \mathrm{PC}(d,y)\mathrm{PC}(d+l,y)}{\sqrt{\sum_{y=1}^{N-1} \mathrm{PC}(d,y)^2 \sum_{y=1}^{N-1} \mathrm{PC}(d+l,y)^2}}, \quad (1)$$

where PC(t) has been converted to a function of day of the year (d) and lag days (l), and N is the number of years of the data. The $\mathrm{ACF}(d,l)$ is then smoothed over a 181-day window along the d axis (to smoothen daily fluctuations) using a Gaussian filter with a full width at half maximum of 42 days (standard deviation of 8 days). Finally, for each d, an exponential curve is fitted to the smoothed $\mathrm{ACF}(l)$ up to a lag of 50 days using the least squares method. An e-folding time scale (τ) is then derived for a given d, representing the time at which the exponential fit of the ACF decreases to e^{-1} (Fig. 1c).

We found that the estimation of $\tau(d)$ exhibits some sensitivity to the length of the data record. To provide a measure of sampling uncertainty in the ERA5, we perform 1,000 times of bootstrap resampling, each time redrawing all yearly $\mathrm{PC}(d,y)$ with replacement to form a new sample as large as the original sample size (same number of total years). Repeating the above ACF calculation for all bootstrap samples leads us to 1,000 values of τ for a given day (Fig. 1c). The distribution of these values provides the possible range of the estimated $\tau(d)$.

https://doi.org/10.5194/egusphere-2025-666
Preprint. Discussion started: 21 February 2025

Note that we perform the EOF analysis separately for each dataset to identify SAM as the leading mode within each simulation, allowing for potential differences in its spatial structure across models.

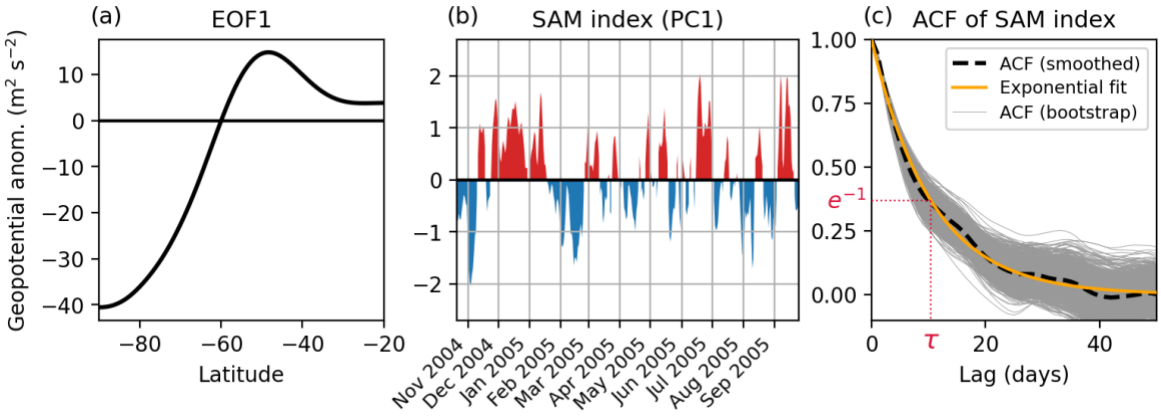

Figure 1. Example of the SAM decorrelation timescale calculation based on ERA5: (a) The first EOF pattern; (b) Associated first PC1 time series (only a partial segment is shown here); (c) Autocorrelation function (ACF) of the SAM index (smoothed with a Gaussian filter) shown for a given day of the year (black dashed), and an exponential fit (yellow). The e-folding timescale is denoted as τ. The ACF is repeated 1,000 times (gray) with the bootstrap sampling with replacement.

3.2 Tropospheric westerly jet position

The westerly jet is diagnosed following Bracegirdle et al. (2020) based on the monthly mean zonally averaged 850-hPa zonal wind. The latitude where the maximum value is found between 75°S and 10°S defines the position of tropospheric westerly jet, λ_0.

3.3 Contribution of atmospheric eddy feedback strength to SAM persistence

In the literature, various methods have been proposed to assess the strength of tropospheric eddy-mean flow feedback. We adopt the approach of Simpson et al. (2013b), as it has been successfully applied to potentially explain the SAM persistence bias in CMIP5 models. This approach estimates the contribution of eddy momentum flux convergence to the tendency of SAM-associated westerly wind anomalies. Therefore, within this framework, SAM is alternatively (but physics-consistently) described

https://doi.org/10.5194/egusphere-2025-666
Preprint. Discussion started: 21 February 2025

by the first EOF of vertically averaged (pressure weighted) zonal-mean zonal wind anomalies, deseasonalized and detrended, over 20-90°S. The resultant EOF latitudinal pattern (**e**) and associated PC time series are defined such that the former has units of m s^{-1}, the latter has unit variance, and their multiplication reconstructs the SAM-associated (EOF1) zonal wind anomaly fields in latitude and time space. For simplicity and consistency with Simpson et al. (2013b) in their CMIP5 assessment, only three pressure levels of 850, 500, 250 hPa are utilized for calculating this diagnostic.

A quantity or a forcing term (denoted as X as an example) associated with the SAM is derived by projecting it onto the EOF pattern (**e**) with the operator:

$$[\bar{X}]_s = \frac{[\bar{\mathbf{X}}]\mathbf{We}}{\sqrt{\mathbf{e}^\top \mathbf{We}}}, \tag{2}$$

where the overbars denote the zonal mean, brackets indicate the vertical average, $[\bar{\mathbf{X}}]$ is a vector form of $[\bar{X}](\lambda, t)$, where λ and t are latitude and time, and **W** is a matrix with diagonal elements equal to the $\cos(\lambda)$ weighting when defining the EOF in Simpson et al. (2013b). The resultant $[\bar{X}]_s$ is a time series. How strongly the eddy forcing sustains the SAM wind anomalies is then estimated by projecting the vertically and zonally averaged zonal momentum tendency equation onto **e**:

$$\frac{\partial [\bar{u}]_s}{\partial t} = [\bar{m}]_s + [\bar{F}]_s, \tag{3}$$

$$[\bar{m}]_s = -\left[\frac{1}{a\cos^2\lambda}\frac{\partial(\overline{u'v'}\cos^2\lambda)}{\partial\lambda}\right]_s, \tag{4}$$

where $[\bar{m}]_s$ is the eddy momentum flux convergence attributed to SAM, u' and v' are the deviation of the zonal and meridional velocities from their zonal means, respectively, and are calculated based on the instantaneous fields at 6-hourly intervals before being converted to daily means, a is the Earth radius, and $[\bar{F}]_s$ represents all the residual momentum forcing associated with SAM. Note that Equation (3) assumes that the sum of individual projected forcing terms on the right-hand side is in balance with the tendency of the SAM anomalies. While this assumption may not be strictly mathematically valid, Simpson et al. (2013b) demonstrated that it holds in their simulations.

Lorenz and Hartmann (2001) hypothesized that the eddy forcing of the SAM consists of a random component and a feedback component that depends linearly on the pre-existing state of SAM, $[\bar{m}]_s =$

https://doi.org/10.5194/egusphere-2025-666
Preprint. Discussion started: 21 February 2025

$\tilde{m} + b[\bar{u}]_s$, where b denotes the eddy feedback strength. To obtain b, Simpson et al. (2013b) performed the lagged linear regressions of $[\bar{m}]_s$ and $[\bar{u}]_s$ onto the SAM index PC(t), such that for a lag day l, $[\bar{m}]_s(t+l) \approx \beta_m(l)PC(t)$ and $[\bar{u}]_s(t+l) \approx \beta_u(l)PC(t)$, where β_m and β_u are the regression coefficients. Accordingly, the eddy forcing of SAM at lag l, $[\bar{m}]_s(t+l)$, can be expressed as $\beta_m(l)PC(t) = \beta_{\tilde{m}}(l)PC(t) + b\beta_u(l)PC(t)$. Assuming that at sufficiently large positive lags, the feedback component dominates the eddy forcing, i.e., $\beta_{\tilde{m}} \approx 0$, we can estimate the eddy feedback strength as a function of lag days (l) by

$$b(l) = \frac{\beta_m(l)}{\beta_u(l)}.$$

In Simpson et al. (2013b), the b averaged over lags from 7 to 14 days is used to denote the eddy feedback strength contributing to the SAM for the intercomparison of the models.

3.4 Contribution of surface wind stress to SAM persistence

While the eddy momentum flux convergence primarily contributes positively to the persistence of SAM, it is counteracted by the negative impacts, predominantly driven by the surface friction (appears as a subcomponent of $[\bar{F}]_s$ in Equation (3)), which acts to dissipate the SAM anomalies. Since the friction term for the zonal wind tendency is not directly available from the phase 1 EERIE simulation outputs, we infer its impact from the surface wind stress in the eastward direction. This variable, $metss$ (or avg_iews as renamed in the ECMWF encoding), represents the daily mean eastward turbulent surface stress resulting from turbulent atmospheric eddies near the surface (due to the roughness of the surface) and turbulent orographic form drag, represented in units of N m^{-2}. Positive values of $metss$ indicate that the air flowing over the surface exerts stress directed toward the East, which translates into a westward frictional force acting on the wind, slowing down the eastward wind tendencies.

Following a similar approach for calculating $[\bar{m}]_s$, we multiplied $metss$ by -1 and projected it onto the EOF pattern ($\mathbf{e}$) as in Equation (2) to estimate the frictional forcing for the SAM zonal wind anomalies, denoted as $[\bar{f}]_s$. Note that $[\bar{f}]_s$ does not have the same physical units as $[\bar{m}]_s$ or $\frac{\partial[\bar{u}]_s}{\partial t}$ (unit: m s^{-2}), and thus cannot be quantitatively compared with $[\bar{m}]_s$. Still, it is useful for the intercomparison among IFS-AMIP idealized experiments to examine whether the surface friction causing the SAM dissipation

https://doi.org/10.5194/egusphere-2025-666
Preprint. Discussion started: 21 February 2025

mechanism is affected by the presence of ocean mesoscales features (specifically their direct thermodynamic forcing) in the SST field.

4. Results

4.1 Model performance for SAM persistence

Figure 2 compares the performance of EERIE and CMIP6 models in representing SAM persistence, measured by the decorrelation time scale (τ). Consistent with Bracegirdle et al. (2020), CMIP6 models tend to overestimate SAM persistence compared to the reanalysis data analyzed over the same historical period (1980–2014). On the annual mean, CMIP6 presents a median value of 11 days, while the ERA5 shows a τ of 8 days. Systematically positive biases in τ seems to persist in the EERIE coupled simulations, with a median value of 10 days. However, it should be noted that most of these simulations are run under a pre-industrial 1850s' or 1950s' forcing (even the IFS-FESOM2 historical simulation is only available for 1950–1969). The Southern Hemisphere circulation and the SAM can change over time, influenced by multiple factors such as the stratospheric ozone depletion and recovery, ENSO variability, changes in sea-ice extent and more. While our analysis of the SAM has removed the seasonal cycle and long-term trends, some non-stationary features may remain, leading to a varying τ depending on the analysis periods. Indeed, the EERIE median value is much closer to the earlier-period (1958–1978) ERA5 result of 10.3 days, with biases that are smaller and more evenly distributed on both sides.

During the austral early summer (NDJ), the overestimation of SAM persistence in CMIP6 is more pronounced with a longer tail of τ distribution. The maximum and median τ in CMIP6 is 32 days and 16 days, respectively, compared to the ERA5 value of 11 days for the same historical period. Compared to CMIP6, EERIE coupled simulations exhibit some noticeable improvement with the maximum and median value of 17 days and 14 days, respectively. Again, such a distribution is even less biased when compared to the earlier-period ERA5 (τ of 16 days).

Interestingly, the atmosphere-only EERIE simulations (IFS-AMIP) overall outperform the ocean-coupled runs with a smaller spread of τ, suggesting that the historical SST boundary condition serves a

https://doi.org/10.5194/egusphere-2025-666
Preprint. Discussion started: 21 February 2025

good physical constraint on the SAM persistence. With all five members considered, the simulated τ at 28 km is still positively biased for both annual and austral-summer means, but the biases do not exceed more than 4.5 days and at least one member presents almost identical values (8 days annually and 11 days in NDJ) to ERA5. Refining the atmospheric resolution from 28 km to 9 km lowers the SAM decorrelation timescale to become slightly negatively biased (8 days annually and 10 days in NDJ) although they are still within the measurement uncertainty ranges of ERA5.

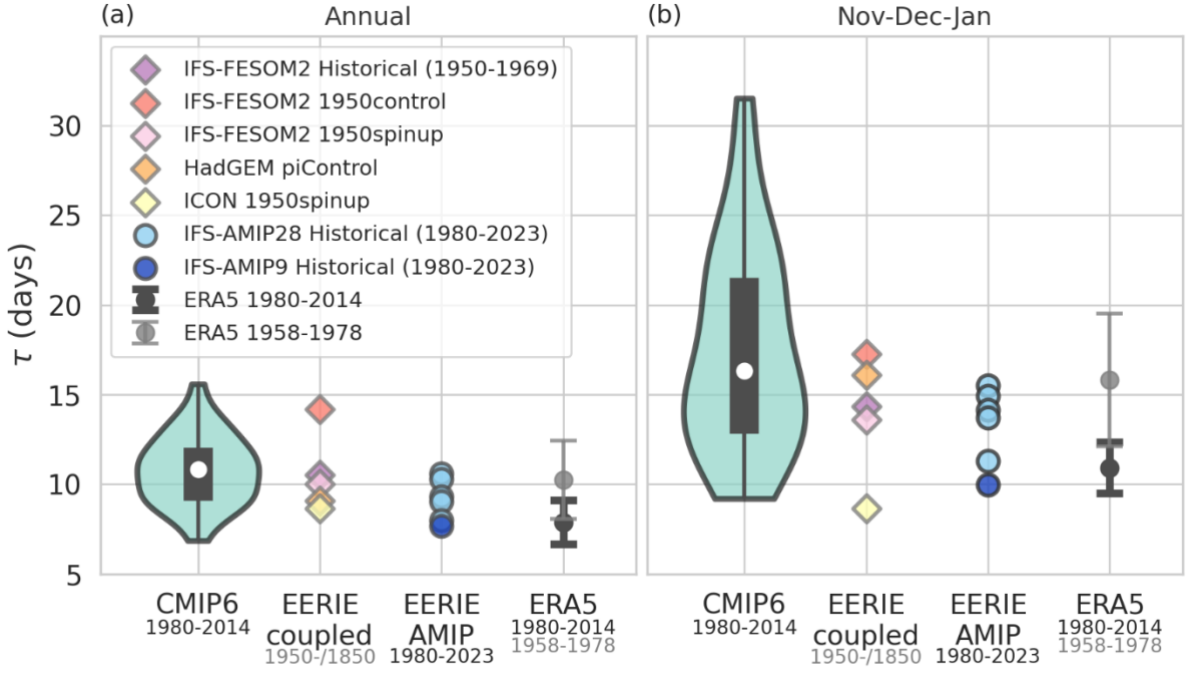

Figure 2. Distribution of simulated τ (days) in CMIP6, EERIE coupled, and EERIE atmosphere-only (AMIP) simulations. The simulations from CMIP6 and EERIE AMIP are both historical, with their period indicated in the x-axis labels, and the simulations from EERIE coupled vary as indicated in Table 1. ERA5 is analyzed for two time periods as references for the historical and pre-industrial periods, both expressed in error bars showing the ±1 standard deviation of the results from the 1,000 bootstrap samples.

4.2 The relationship between jet location and τ

The relationship between westerly jet location (λ_0) and SAM decorrelation timescale (τ) is then re-visited. Similar to their predecessors, CMIP6 models show a positive correlation between λ_0 and τ, that

https://doi.org/10.5194/egusphere-2025-666
Preprint. Discussion started: 21 February 2025

is, models with a more equatorward jet location tend to exhibit a more persistent SAM. Consistent with Simpson & Polvani's (2016) result based on CMIP5 models, the slope of the linear fit is larger during NDJ, indicating a larger variation in τ given the same variation in λ_0 during this season. Examining the model resolution of each CMIP6 simulation, there appears no strong or clear relationship between the model resolution and the model biases in these two quantities (same for both latitudinal and longitudinal resolutions and for both atmosphere and ocean models, although only the atmospheric latitudinal resolution is expressed in Fig. 3). A potential dependency on resolution could be obscured in the CMIP6 ensemble by other cancelling factors, which vary from simulations incorporating different configurations and model systems. However, it is also possible that the importance of resolution (or the improvements attributed to a higher resolution) in determining the performance of the large-scale SAM variability and mean jet has reached a plateau with the typical grid size reached in the current GCMs (CMIP6) and other factors are becoming more critical. For instance, based on simplified atmospheric GCMs with idealized forcing, Gerber et al. (2008) found that the decorrelation timescale of the annular mode is unrealistically large at a coarse resolution of T21 (5.6°). While such a bias was notably reduced by refining the model resolution to T42 (2.8°), no further improvement was shown with a model resolution higher than T42 and the τ converges to a still positively biased value.

On the annual mean, EERIE simulations generally fall within a region smaller than that covered by CMIP6, with the IFS-FESOM control being the worst performing experiment among the EERIE simulations (Fig. 3a), showing both the greatest positive bias in τ and λ_0. For NDJ, a clear improvement of EERIE models in representing the SAM persistence is again shown as the spread of EERIE clearly shifts toward a lower τ, closer to ERA5's τ compared to other CMIP6 exhibiting a similar jet location. In all, a positive λ_0-τ relationship remains across EERIE models (Fig. 3). However, the slope of the linear fit is greater for annual means than for early summer, mainly because of the specific behavior of the IFS-FESOM control. The most skillful EERIE simulations for the SAM persistence, IFS-AMIP, all well capture the jet location (with a bias $< 1°$). This highlights again the importance of well-represented sea surface features to the large-scale atmospheric circulation and variability. Still, even with the same IFS model and the same 28-km grid size, the five IFS-AMIP ensemble members generated by perturbing the initial conditions (the only difference is the internal variability) exhibits a spread in τ of

https://doi.org/10.5194/egusphere-2025-666
Preprint. Discussion started: 21 February 2025

about 5 days, which is not positively correlated with the corresponding simulated jet location. This result suggests that the documented bias relationship between τ and λ_0 in the literature does not always hold, particularly in our IFS-AMIP setup with prescribed SSTs. It is also possible that when the jet location is relatively well-captured, other factors become increasingly important to influence the persistence of SAM, and we explore some of these potential factors in the next section using idealized sensitivity experiments.

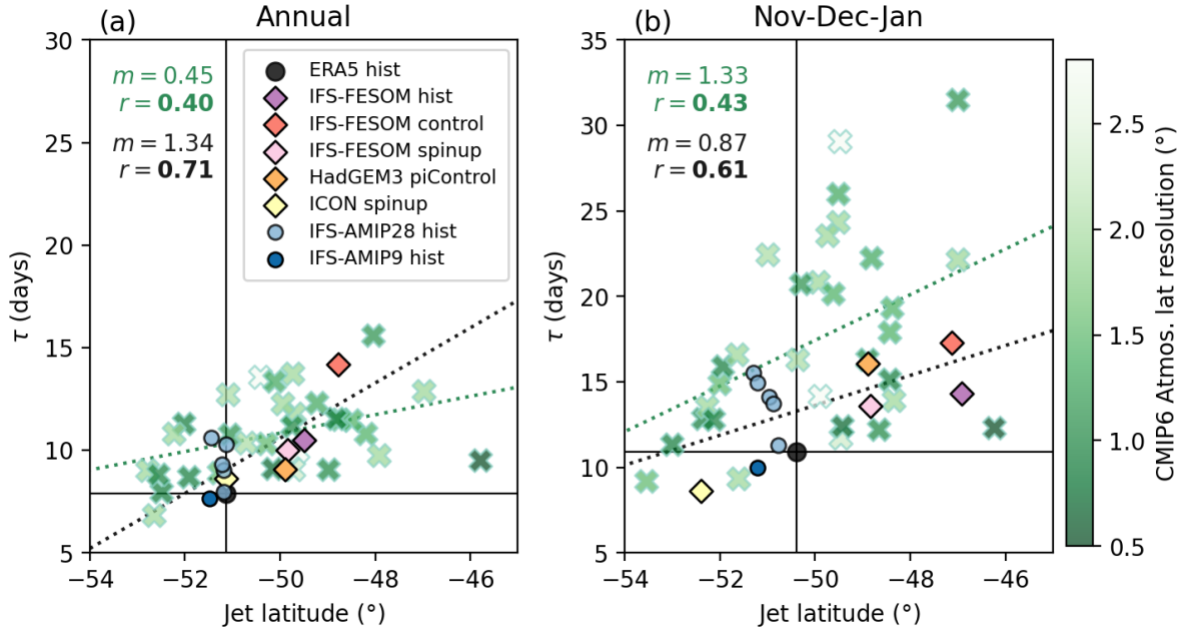

Figure 3. Scatter plot of climatological jet latitude (°) versus SAM decorrelation timescale τ (days) for (a) annual and (b) early-summer (NDJ) means in the Southern Hemisphere. Green crosses are based on CMIP6 historical simulations (colored by the latitudinal resolution in their atmospheric model). ERA5 reanalysis and EERIE simulations are indicated as in the legend. Vertical and horizontal lines are the ERA5 values. The green dotted straight line is the linear least-squares regression fit for CMIP6 models (slope is denoted as *m*, and Pearson correlation coefficient *r* is expressed in bold if statistically significant with the *p* value <0.05 in green in the top left corner). Similarly, the black dotted line is the linear fit for all EERIE simulations.

4.3 Sensitivities to varying SST boundary conditions

EERIE simulations demonstrate a reduced bias in summer-time SAM persistence compared to CMIP6, but identifying the cause is challenging due to variability in model systems. Although CMIP6 results show no clear link between model resolution and performance in τ and λ_0, the higher resolution in

https://doi.org/10.5194/egusphere-2025-666
Preprint. Discussion started: 21 February 2025

EERIE remains one possible contributing factor to such an improvement. One piece of evidence is the reduction in τ when transitioning from a 28-km to a 9-km model grid size using a consistent IFS model. Another possibility is that the new generation of models in EERIE improve model physics, reducing the biases in processes that resulted in a too-persistent SAM in earlier CMIP-like GCMs. In addition, EERIE begins to explicitly resolve the ocean mesoscales, which are parameterized in CMIP6, though the resulting impacts on SAM persistence have not been investigated. To explore these possibilities, this section focuses on EERIE atmosphere-only sensitivity experiments with varied SST boundary conditions, aiming to investigate the influence of ocean mesoscales and model resolution in the observed improvement within a controlled framework.

We first focus on the 28-km simulations. Regarding the seasonal variation of τ (Fig. 4a), the experiments in which ocean mesoscales are removed (either NoEddies or NoFronts) exhibit intermingled patterns overlapping with those of ObsSST. However, their ensemble means suggest a slight reduction in τ (by approximately 2 days) during NDJ. This result indicates that the presence of ocean mesoscale SST features, whether quasi-stationary or transient, helps sustain SAM persistence (hence the larger τ in the ensemble mean of ObsSST) during this period. All these 28-km experiments show a slightly poleward biased jet latitude compared to ERA5 (within 1°) during NDJ, and the ensemble mean of ObsSST is the least biased compared to those of NoEddies and NoFronts (Fig. 4b). While this seems to be in agreement with the literature that a more southward-shifted jet is associated with a longer SAM persistence, there is an overall small and even negative correlation between the λ_0 and τ of -0.22 considering all IFS-AMIP simulations.

In contrast, the eddy feedback strength b appears a better indicator for SAM persistence, exhibiting a correlation coefficient with τ of 0.47 with a p-value of 0.08 (Fig. 4c). While the p-value does not meet the conventional threshold for statistical significance ($p<0.05$), it is notably lower than the examined λ_0-τ relationship (p-value 0.42). However, the difference of b among different sets of SST-boundary-condition experiments cannot explain solely the observed reduction of SAM persistence in both NoEddies and NoFronts. Specifically, while the ensemble mean of NoEddies shows a slightly weaker b than that of ObsSST, NoFronts show values similar with or even larger than ObsSST.

https://doi.org/10.5194/egusphere-2025-666
Preprint. Discussion started: 21 February 2025

We then examine the surface frictional effects on SAM in these simulations (Fig. 4d), and no clear difference in $[\bar{f}]_s$ is found among ObsSST, NoEddies, and NoFronts. Experiments ObsSST and NoFronts exhibit highly similar values, while NoEddies exhibit a large ensemble spread and a slightly larger ensemble-mean value. A closer examination shows that the member in NoEddies with the largest value in $[\bar{f}]_s$ is accompanied by the weakest eddy feedback b (red cross markers in Fig. 4c-d) and vice versa (red square markers). The opposite shifts of these two dominant mechanisms indicates an offset between each other, which explains why these members with the largest magnitudes of $[\bar{f}]_s$ do not appear as outliers in the distribution of SAM persistence. However, the quantification of the net effects of eddy forcing and surface friction requires a comprehensive budget analysis.

The potential impact from ocean mesoscale on the SAM persistence is, however, not observed in the 9 km simulations, as NoEddies shows almost no change from ObsSST in τ (Fig. 4e). That said, one ensemble member may be not enough to identify the influence of the ocean eddies as the τ fluctuation is quite large among the 28-km ensemble members, even given the same SST boundary condition. For the other metrics, the single runs of 9 km qualitatively align with the ensemble means of 28-km simulations: The suppression/filtering of ocean eddies in SST boundaries leads to a slight poleward shift (more biased than ObsSST) of the mean-state jet, a weaker eddy feedback sustaining the SAM anomalies, and a slightly reduced surface frictional impact dissipating SAM. The same signs of changes in the latter two counteracting mechanisms render their net impact on sustaining SAM uncertain. It is possible that the changes in these two processes, influenced by the presence of ocean eddies, counterbalance each other at 9 km, resulting in a comparable τ between NoEddies and ObsSST. However, these analyses do not clearly account for the significant reduction in τ when the model grid size is refined from 28 km to 9 km, as all three diagnostics indicate that the 9-km simulation falls within the range of values covered by the 28-km simulations. Additional simulations and diagnostics would be required to confirm the underlying cause for the observed model grid spacing dependency.

https://doi.org/10.5194/egusphere-2025-666
Preprint. Discussion started: 21 February 2025

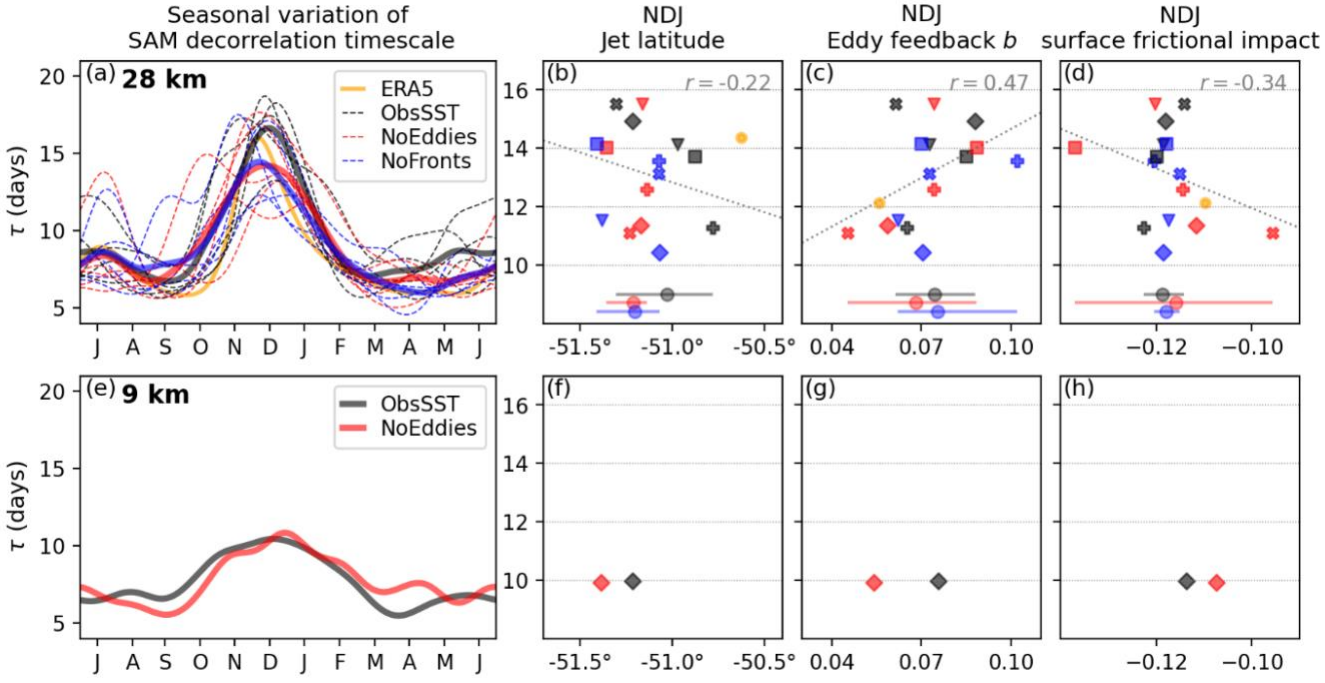

Figure 4. (a) SAM decorrelation timescale (τ) as a function of month for IFS-AMIP 28km simulations (dashed lines for ensemble members and solid lines for the ensemble means; experiments indicated in the legend) and ERA5 (yellow). (b) Scatter plot of τ (days) and westerly jet latitude (each marker for one simulation; the horizontal bar in the bottom shows the minimum- to maximum- range with the circle for the ensemble mean of each set of the SST experiments). (c)–(d) Similar to (b) but for the eddy feedback strength and frictional effects associated with SAM, respectively. In (b)–(d), the gray dotted line represents the linear regression fit and the correlation coefficient is indicated in the top-right corner. (e)–(h) Same as (a)–(d), but for the 9-km simulations.

5 Discussion and conclusions

This study assesses the performance of new high-resolution global model simulations developed under the EERIE project in capturing the persistence of the Southern Annular Mode (SAM), a key driver of climate variability in the Southern Hemisphere. EERIE simulations are conducted with a model grid size of 9–28 km for the atmosphere and 5–13 km for the ocean. The persistence of the SAM is assessed using the decorrelation timescale of the SAM index (τ), for which CMIP GCMs have historically exhibited a systematic positive bias (overly persistent) in austral summer, often correlated with a climatological westerly jet that is too equatorward. Our conclusions and discussion based on the phase 1

https://doi.org/10.5194/egusphere-2025-666
Preprint. Discussion started: 21 February 2025

preliminary simulations of the EERIE models are organized into two subsections: (1) the performance of coupled simulations, and (2) the performance of atmosphere-only (AMIP) simulations and insights obtained from the sensitivity experiments with varied SST boundary conditions under the AMIP setup.

5.1 EERIE Coupled simulations

Compared to CMIP6, the EERIE coupled simulations show a slight improvement in representing SAM persistence on an annual-mean basis and a notable advancement in early summer (NDJ). The annual-mean τ distribution in the EERIE coupled simulations (median: 10 days) is similar to that in the CMIP6 historical simulations (median: 11 days), both are positively biased compared to the ERA5 value of 8 days for 1980–2014. Notably, the EERIE simulations primarily represent the earlier 1850s or 1950s period, for which reanalysis suggest a higher τ of 10 days. For early summer (NDJ), the EERIE simulations demonstrate τ values ranging from 9 to 17 days (median: 14 days), in contrast to CMIP6's overestimated range of 9 to 32 days (median: 16 days). This clear improvement of the EERIE simulations for early summer τ holds regardless of the two reference periods used for ERA5 (11 days for the historical period as in CMIP6 and 16 days for an earlier period of 1958-1978).

The relationship between the westerly jet location (λ_o) and τ remains positively correlated in EERIE simulations as has been found for CMIP-like models. Consistently, the smaller bias for τ in EERIE simulations during the austral summer is accompanied by a smaller range of λ_o (closer to ERA5) compared to CMIP6. However, the outperformance for τ in EERIE models compared to the CMIP6 runs that capture similar jet locations indicates other factors in play. Among CMIP6, model resolution shows weak dependency on biases in either λ_o or τ, but it is possible that the impact of resolution is outweighed by other factors varying in CMIP6 simulations incorporating different configurations and model systems.

5.2 EERIE Atmosphere-only simulations

Among EERIE simulations, the IFS-AMIP runs with prescribed historical SST and sea ice boundary conditions show the optimal performance in both SAM persistence and westerly jet location, with smaller spreads and closer values to ERA5 than the coupled runs. This highlights the importance of

https://doi.org/10.5194/egusphere-2025-666
Preprint. Discussion started: 21 February 2025

accurately representing sea surface thermal conditions to improve the simulation of these large-scale atmospheric quantities. While some studies have demonstrated that the air-sea coupling is critical in modulating the SAM (although they focused on interseasonal scales, longer than the intraseasonal scale being investigated here; Sen Gupta and England, 2006), our results suggest that the atmosphere-ocean coupling plays a secondary role relative to the SST biases introduced by the coupling, an ongoing challenge common to ocean-atmosphere coupled GCMs (Zhang et al., 2023). Notably, the IFS-AMIP historical simulations significantly reduce biases compared to CMIP6, with errors of less than 4.5 days in τ and 1° in λ_o with respect to ERA5.

For the AMIP historical simulations, the λ_o–τ bias relationship does not apply, as the approximately 5-day ensemble spread in τ shows no positive correlation with the minimally varying λ_o. It is possible that when the jet location is already well-captured, other factors become increasingly important for the persistence of SAM. Especially, the impact of resolution stands out and can be more clearly interpreted using the same model. Refining the IFS model grid size from 28 km to 9 km lowers the simulated τ to even lower than the ERA5 value, although it is worth noting that ERA5 has a resolution closer to 28 km.

The potential importance of ocean mesoscale features is explored via idealized AMIP experiments. Taking the historical runs as reference (ObsSST experiment), two experiments are carried out by filtering out the quasi-stationary ocean fronts (NoFronts experiment) or the transient ocean eddies (NoEddies) in the SST boundary conditions. While three experiments (each with five ensemble members) at 28 km show intertangled seasonal variations of τ, their ensemble means suggest that the presence of ocean mesoscales, regardless of fronts or eddies, may help to maintain the SAM anomalies increasing the persistence by roughly 2 days in early summer. However, such an effect is not captured in the 9-km simulations, although there is only one ensemble member for each experiment. Purich et al. (2021) performed similar experiments but with a coupled GCM, ACCESS1.0, to explore the role of oceanic variability on SAM by restoring the SST to the monthly mean patterns. They found that suppressing Southern Ocean SST variability does not impact SAM persistence in their simulations, but their analysis was on monthly rather than daily means and with a coarser model resolution of ~130 km.

https://doi.org/10.5194/egusphere-2025-666
Preprint. Discussion started: 21 February 2025

As they concluded, eddy-resolving models are required to properly capture the air–sea feedbacks in the Southern Hemisphere.

Using the idealized AMIP experiments, we conduct further exploration on the "internal" atmospheric dynamical mechanisms contributing to the SAM persistence, eddy feedback strength and surface friction. It is worth noting that the eddy feedback strength appears to be a better indicator than the mean-state jet latitude λ_0, linking positively and more statistically significantly to the simulated summertime τ among the IFS AMIP simulations. Still, by how much it is counteracted by the surface friction requires a more comprehensive budget analysis. Likely because of those compensating effects, the metrics of jet latitude, eddy feedback and frictional impact, do not provide a clear answer as to what contribute to the observed differences in the simulated τ when ocean mesoscales are removed.

This result highlights the complexity of mechanisms contributing to the SAM persistence in GCMs. For instance, the interplay between eddy forcing and surface friction suggests that even small errors in one process may result in notable uncertainty in their net impact. Additionally, this study only considers the zonally averaged properties, but non-zonal components likely play important roles in shaping SAM characteristics in climate systems and hence their representation in GCMs (e.g., Barnes and Hartmann, 2010; Sen Gupta and England, 2006). Nevertheless, the general improvements seen in the phase 1 simulations of the EERIE coupled models present a promising path forward in addressing the long-standing GCM biases in SAM persistence, especially considering the challenges in optimally configuring high-resolution models (i.e., tuning) and the lack of community experience in doing so. Furthermore, the controlled framework of the IFS-AMIP idealized eddy-rich experiments offers significant potential for enhancing our understanding of atmospheric responses to ocean mesoscales.

Acknowledgments

This publication is part of the EERIE project funded by the European Union. Views and opinions expressed are however those of the author(s) only and do not necessarily reflect those of the European Union or the European Climate Infrastructure and Environment Executive Agency (CINEA). Neither the European Union nor the granting authority can be held responsible for them. This work has received funding from the Swiss State Secretariat for Education, Research and Innovation (SERI) under contract

https://doi.org/10.5194/egusphere-2025-666
Preprint. Discussion started: 21 February 2025

#22.00366. This work was funded by UK Research and Innovation (UKRI) under the UK government's Horizon Europe funding guarantee (grant number 10057890, 10049639, 10040510, 10040984). Hugues Goosse is Research Director with the Fonds de la Recherche Scientifique (F.R.S. -FNRS). The authors also thank Francesco Ragone, Isla Simpson, Matthew Patterson, Thomas Bracegirdle for providing constructive suggestions or clarification about the methodologies employed in their works.

Data Availability Statement

All EERIE simulation outputs are publicly accessible at https://eerie.cloud.dkrz.de and Wachsmann et al. (2024). The calculation of EOFs was performed using the publicly available Python package by Dawson (2016). All scripts used for the analysis and figure generation will be shared in the GitHub repository under the EERIE project (https://github.com/eerie-project) upon acceptance of the publication.

References

Barnes, E.A., Hartmann, D.L., 2010. Dynamical Feedbacks of the Southern Annular Mode in Winter and Summer. J. Atmospheric Sci. 67, 2320–2330. https://doi.org/10.1175/2010JAS3385.1

Bracegirdle, T.J., Holmes, C.R., Hosking, J.S., Marshall, G.J., Osman, M., Patterson, M., Rackow, T., 2020. Improvements in Circumpolar Southern Hemisphere Extratropical Atmospheric Circulation in CMIP6 Compared to CMIP5. Earth Space Sci. 7, e2019EA001065. https://doi.org/10.1029/2019EA001065

Busecke, J.J.M., Abernathey, R.P., 2019. Ocean mesoscale mixing linked to climate variability. Sci. Adv. 5, eaav5014. https://doi.org/10.1126/sciadv.aav5014

Campitelli, E., Díaz, L.B., Vera, C., 2022. Assessment of zonally symmetric and asymmetric components of the Southern Annular Mode using a novel approach. Clim. Dyn. 58, 161–178. https://doi.org/10.1007/s00382-021-05896-5

Chassignet, E.P., Xu, X., 2021. On the Importance of High-Resolution in Large-Scale Ocean Models. Adv. Atmospheric Sci. 38, 1621–1634. https://doi.org/10.1007/s00376-021-0385-7

Codron, F., 2005. Relation between Annular Modes and the Mean State: Southern Hemisphere Summer. J. Clim. 18, 320–330. https://doi.org/10.1175/JCLI-3255.1

Dawson, A., 2016. eofs: A Library for EOF Analysis of Meteorological, Oceanographic, and Climate Data. J. Open Res. Softw. 4, 14. https://doi.org/10.5334/jors.122

Ding, Q., Steig, E.J., Battisti, D.S., Wallace, J.M., 2012. Influence of the Tropics on the Southern Annular Mode. J. Clim. 25, 6330–6348. https://doi.org/10.1175/JCLI-D-11-00523.1

https://doi.org/10.5194/egusphere-2025-666
Preprint. Discussion started: 21 February 2025

Doddridge, E.W., Marshall, J., 2017. Modulation of the Seasonal Cycle of Antarctic Sea Ice Extent Related to the Southern Annular Mode. Geophys. Res. Lett. 44, 9761–9768. https://doi.org/10.1002/2017GL074319

European Commission, 2022. European Eddy-RIch ESMs [WWW Document]. URL https://doi.org/10.3030/101081383 (accessed 2.2.25).

Eyring, V., Bony, S., Meehl, G.A., Senior, C.A., Stevens, B., Stouffer, R.J., Taylor, K.E., 2016. Overview of the Coupled Model Intercomparison Project Phase 6 (CMIP6) experimental design and organization. Geosci. Model Dev. 9, 1937–1958. https://doi.org/10.5194/gmd-9-1937-2016

Fogt, R.L., Marshall, G.J., 2020. The Southern Annular Mode: Variability, trends, and climate impacts across the Southern Hemisphere. WIREs Clim. Change 11, e652. https://doi.org/10.1002/wcc.652

Gerber, E.P., Baldwin, M.P., Akiyoshi, H., Austin, J., Bekki, S., Braesicke, P., Butchart, N., Chipperfield, M., Dameris, M., Dhomse, S., Frith, S.M., Garcia, R.R., Garny, H., Gettelman, A., Hardiman, S.C., Karpechko, A., Marchand, M., Morgenstern, O., Nielsen, J.E., Pawson, S., Peter, T., Plummer, D.A., Pyle, J.A., Rozanov, E., Scinocca, J.F., Shepherd, T.G., Smale, D., 2010. Stratosphere-troposphere coupling and annular mode variability in chemistry-climate models. J. Geophys. Res. Atmospheres 115, 2009JD013770. https://doi.org/10.1029/2009JD013770

Gerber, E.P., Voronin, S., Polvani, L.M., 2008. Testing the Annular Mode Autocorrelation Time Scale in Simple Atmospheric General Circulation Models. Mon. Weather Rev. 136, 1523–1536. https://doi.org/10.1175/2007MWR2211.1

Gillett, N.P., Kell, T.D., Jones, P.D., 2006. Regional climate impacts of the Southern Annular Mode. Geophys. Res. Lett. 33, 2006GL027721. https://doi.org/10.1029/2006GL027721

Haarsma, R.J., Roberts, M.J., Vidale, P.L., Senior, C.A., Bellucci, A., Bao, Q., Chang, P., Corti, S., Fučkar, N.S., Guemas, V., Von Hardenberg, J., Hazeleger, W., Kodama, C., Koenigk, T., Leung, L.R., Lu, J., Luo, J.-J., Mao, J., Mizielinski, M.S., Mizuta, R., Nobre, P., Satoh, M., Scoccimarro, E., Semmler, T., Small, J., Von Storch, J.-S., 2016. High Resolution Model Intercomparison Project (HighResMIP v1.0) for CMIP6. Geosci. Model Dev. 9, 4185–4208. https://doi.org/10.5194/gmd-9-4185-2016

Hersbach, H., Bell, B., Berrisford, P., Hirahara, S., Horányi, A., Muñoz-Sabater, J., Nicolas, J., Peubey, C., Radu, R., Schepers, D., Simmons, A., Soci, C., Abdalla, S., Abellan, X., Balsamo, G., Bechtold, P., Biavati, G., Bidlot, J., Bonavita, M., De Chiara, G., Dahlgren, P., Dee, D., Diamantakis, M., Dragani, R., Flemming, J., Forbes, R., Fuentes, M., Geer, A., Haimberger, L., Healy, S., Hogan, R.J., Hólm, E., Janisková, M., Keeley, S., Laloyaux, P., Lopez, P., Lupu, C., Radnoti, G., De Rosnay, P., Rozum, I., Vamborg, F., Villaume, S., Thépaut, J., 2020. The ERA5 global reanalysis. Q. J. R. Meteorol. Soc. 146, 1999–2049. https://doi.org/10.1002/qj.3803

Hewitt, H.T., Roberts, M., Mathiot, P., Biastoch, A., Blockley, E., Chassignet, E.P., Fox-Kemper, B., Hyder, P., Marshall, D.P., Popova, E., Treguier, A.-M., Zanna, L., Yool, A., Yu, Y., Beadling, R., Bell, M., Kuhlbrodt, T., Arsouze, T., Bellucci, A., Castruccio, F., Gan, B., Putrasahan, D., Roberts, C.D., Van Roekel, L., Zhang, Q., 2020. Resolving and Parameterising the Ocean Mesoscale in Earth System Models. Curr. Clim. Change Rep. 6, 137–152. https://doi.org/10.1007/s40641-020-00164-w

https://doi.org/10.5194/egusphere-2025-666
Preprint. Discussion started: 21 February 2025

Ho, M., Kiem, A.S., Verdon-Kidd, D.C., 2012. The Southern Annular Mode: a comparison of indices. Hydrol. Earth Syst. Sci. 16, 967–982. https://doi.org/10.5194/hess-16-967-2012

Karoly, D.J., 1989. Southern Hemisphere Circulation Features Associated with El Niño-Southern Oscillation Events. J. Clim. 2, 1239–1252. https://doi.org/10.1175/1520-0442(1989)002<1239:SHCFAW>2.0.CO;2

Kidston, J., Gerber, E.P., 2010. Intermodel variability of the poleward shift of the austral jet stream in the CMIP3 integrations linked to biases in 20th century climatology. Geophys. Res. Lett. 37, 2010GL042873. https://doi.org/10.1029/2010GL042873

Lefebvre, W., Goosse, H., 2005. Influence of the Southern Annular Mode on the sea ice-ocean system: the role of the thermal and mechanical forcing. Ocean Sci. 1, 145–157. https://doi.org/10.5194/os-1-145-2005

Lenton, A., Matear, R.J., 2007. Role of the Southern Annular Mode (SAM) in Southern Ocean CO_2 uptake. Glob. Biogeochem. Cycles 21, 2006GB002714. https://doi.org/10.1029/2006GB002714

Lim, E.-P., Hendon, H.H., Rashid, H., 2013. Seasonal Predictability of the Southern Annular Mode due to Its Association with ENSO. J. Clim. 26, 8037–8054. https://doi.org/10.1175/JCLI-D-13-00006.1

Loose, N., Abernathey, R., Grooms, I., Busecke, J., Guillaumin, A., Yankovsky, E., Marques, G., Steinberg, J., Ross, A., Khatri, H., Bachman, S., Zanna, L., Martin, P., 2022. GCM-Filters: A Python Package for Diffusion-based Spatial Filtering of Gridded Data. J. Open Source Softw. 7, 3947. https://doi.org/10.21105/joss.03947

Lorenz, D.J., Hartmann, D.L., 2001. Eddy–Zonal Flow Feedback in the Southern Hemisphere. J. Atmospheric Sci. 58, 3312–3327. https://doi.org/10.1175/1520-0469(2001)058<3312:EZFFIT>2.0.CO;2

Lovenduski, N.S., Gruber, N., 2005. Impact of the Southern Annular Mode on Southern Ocean circulation and biology. Geophys. Res. Lett. 32, 2005GL022727. https://doi.org/10.1029/2005GL022727

Purich, A., Boschat, G., Liguori, G., 2021. Assessing the impact of suppressing Southern Ocean SST variability in a coupled climate model. Sci. Rep. 11, 22069. https://doi.org/10.1038/s41598-021-01306-2

Roberts, C., Aengenheyster, M., Roberts, M., 2024a. Description of EERIE atmosphere-only reference simulations. https://doi.org/10.5281/ZENODO.14334612

Roberts, C., Aengenheyster, M., Roberts, M., 2024b. Description of EERIE idealised atmosphere-only simulations. https://doi.org/10.5281/ZENODO.14514510

Roberts, M.J., Jung, T., Ortega, P., Ghosh, R., Wachsmann, F., von Storch, J.-S., Kroeger, J., Aengenheyster, M., Roberts, C., 2024a. Phase 1 simulations, including HighResMIP and CMIP6- PI-control simulations. https://doi.org/10.5281/ZENODO.14288726

Roberts, M.J., Reed, K.A., Bao, Q., Barsugli, J.J., Camargo, S.J., Caron, L.-P., Chang, P., Chen, C.-T., Christensen, H.M., Danabasoglu, G., Frenger, I., Fučkar, N.S., Hasson, S.U., Hewitt, H.T., Huang, H., Kim, D., Kodama, C., Lai, M., Leung, L.-Y.R., Mizuta, R., Nobre, P., Ortega, P., Paquin, D., Roberts, C.D., Scoccimarro, E., Seddon, J., Treguier, A.M., Tu, C.-Y., Ullrich, P.A., Vidale, P.L., Wehner, M.F., Zarzycki, C.M., Zhang, B., Zhang, W., Zhao, M., 2024b. High

https://doi.org/10.5194/egusphere-2025-666
Preprint. Discussion started: 21 February 2025

Resolution Model Intercomparison Project phase 2 (HighResMIP2) towards CMIP7. https://doi.org/10.5194/egusphere-2024-2582

Sen Gupta, A., England, M.H., 2006. Coupled Ocean–Atmosphere–Ice Response to Variations in the Southern Annular Mode. J. Clim. 19, 4457–4486. https://doi.org/10.1175/JCLI3843.1

Simpson, I.R., Hitchcock, P., Shepherd, T.G., Scinocca, J.F., 2013a. Southern Annular Mode Dynamics in Observations and Models. Part I: The Influence of Climatological Zonal Wind Biases in a Comprehensive GCM. J. Clim. 26, 3953–3967. https://doi.org/10.1175/JCLI-D-12-00348.1

Simpson, I.R., Polvani, L.M., 2016. Revisiting the relationship between jet position, forced response, and annular mode variability in the southern midlatitudes. Geophys. Res. Lett. 43, 2896–2903. https://doi.org/10.1002/2016GL067989

Simpson, I.R., Shepherd, T.G., Hitchcock, P., Scinocca, J.F., 2013b. Southern Annular Mode Dynamics in Observations and Models. Part II: Eddy Feedbacks. J. Clim. 26, 5220–5241. https://doi.org/10.1175/JCLI-D-12-00495.1

Son, S. -W., Gerber, E.P., Perlwitz, J., Polvani, L.M., Gillett, N.P., Seo, K. -H., Eyring, V., Shepherd, T.G., Waugh, D., Akiyoshi, H., Austin, J., Baumgaertner, A., Bekki, S., Braesicke, P., Brühl, C., Butchart, N., Chipperfield, M.P., Cugnet, D., Dameris, M., Dhomse, S., Frith, S., Garny, H., Garcia, R., Hardiman, S.C., Jöckel, P., Lamarque, J.F., Mancini, E., Marchand, M., Michou, M., Nakamura, T., Morgenstern, O., Pitari, G., Plummer, D.A., Pyle, J., Rozanov, E., Scinocca, J.F., Shibata, K., Smale, D., Teyssèdre, H., Tian, W., Yamashita, Y., 2010. Impact of stratospheric ozone on Southern Hemisphere circulation change: A multimodel assessment. J. Geophys. Res. Atmospheres 115, 2010JD014271. https://doi.org/10.1029/2010JD014271

Thompson, D.W.J., Solomon, S., Kushner, P.J., England, M.H., Grise, K.M., Karoly, D.J., 2011. Signatures of the Antarctic ozone hole in Southern Hemisphere surface climate change. Nat. Geosci. 4, 741–749. https://doi.org/10.1038/ngeo1296

Wachsmann, F., Matthias Aengenheyster, Wickramage, C., Seddon, J., Nikolay Koldunov, Ziemen, F., 2024. Data access to EERIE ESM output via intake catalogues: Phase1 plus Hackathon simulations. https://doi.org/10.5281/ZENODO.14243677

Zhang, Q., Liu, B., Li, S., Zhou, T., 2023. Understanding Models' Global Sea Surface Temperature Bias in Mean State: From CMIP5 to CMIP6. Geophys. Res. Lett. 50, e2022GL100888. https://doi.org/10.1029/2022GL100888